RESEARCH ARTICLE

ADVANCED OPTICAL MATERIALS
www.advopticalmat.de

Spatially Confined Single-Phosphor Multichromatic Afterglow Based on Cyclodextrin Self-Assembly

*Jinlong Yue, Bo Qiao, Yong Chen, Xu Pan, Xiaolu Zhou, Lihua Wang, and Yu Liu**

There is extensive research interest in sustainable, high-performance persistent luminescent materials, featuring tunable organic afterglow and stimulus responsiveness, owing to their broad application potential. However, despite significant efforts by the scientific community, the value of single-phosphor systems in achieving efficient persistent luminescence through multiple responses is not widely recognized. This work constructs a supramolecular self-assembled system featuring multicolor phosphorescence, fabricated by incorporating (4-(pyridin-4-yl)phenyl)boronic acid (PB3) into a biomass-derived, macrocyclic β-cyclodextrin (β-CD) via multiple intermolecular interactions. Notably, the resulting PB3@β-CD assembly exhibits both excitation-dependent and visible-light excitation capabilities, with an excitation wavelength range spanning 240–420 nm. When excited by white light, the afterglow persists for up to 3 s. Furthermore, the coexistence of isolated and aggregated states of PB3 within the β-CD matrix causes the guest molecules to emit diverse afterglow colors under different excitation conditions. Compared to other matrices, PB3 in the β-CD matrix exhibits blue phosphorescence emission under 260 nm excitation and yellow-green phosphorescence emission under 360 nm excitation. It also maintains phosphorescence emission even at elevated temperatures (162 °C), a rare combination that significantly enhances functional diversity. The responsive nature of the biomass-based system enables the dynamic regulation of room-temperature phosphorescence (RTP) signals, supporting secure data processing.

1. Introduction

Phosphorescent materials that emit light for long periods of time at room temperature, ranging from a few milliseconds to several hours, have attracted much attention in the fields of biomedicals,[1,2] optoelectronic devices,[3] and electronics.[4,5] Most of these molecular structures have been tuned through increasingly sophisticated molecular design principles or crystalline engineering to inhibit nonradiative transitions.[6–9] However, the crystallization process requires a lot of time and very harsh conditions. Desired room-temperature phosphorescent materials typically (1) introduce heteroatoms in conjugated structures containing n-π^* states to facilitate intersystem crossing (ISC) processes;[10–12] (2) create more rigid environments with effective oxygen barrier capabilities,[13,14] including host-guest doping,[15–18] polymerization, supramolecules,[19] and porous frameworks to suppress triple exciton non-radiative attenuation; (3) modulate intermolecular interactions to manipulate molecular stacking achieving suppression of non-radiative attenuation.[20,21]

Organic persistent light-emitting (OPL) materials with tunable emission colors can gather more information and achieve multiple responses through the manipulation of external stimuli, such as mechanical force, heat, light and pH.[22–27] In addition, molecular stacking and spatial arrangement can directly influence intermolecular interactions directly. The resulting J-aggregation, H-aggregation, and the amorphous state aggregation all lead to changes in the color of the afterglow producing concentration dependence and excitation wavelength dependence.[28] There are many strategies for obtaining diverse RTP materials. Substituent engineering is one of the important options.[29–32] However, there are few reports on using of substituent engineering to precisely tune the multicolor of single phosphors, especially for wide-range, tunable, multicolor, efficient RTP materials.[33,34] Herein, we doped guest boronic acid-based compounds into the β-CD biomass host matrix. We utilized substituent engineering to achieve high-performance RTP materials with multi-mode emission, tunable excitation dependence, and visible excitation, using a single phosphor component and modulating the aggregation state (**Scheme 1**). The corresponding doped systems exhibit excitation-dependent afterglow colors and demonstrate phosphorescence behavior at elevated temperatures. This doped system exhibits an exceptionally broad excitation wavelength range (240–420 nm), which is a breakthrough in the field of multi-color luminescence from single

J. Yue, Y. Chen, X. Pan, X. Zhou, L. Wang, Y. Liu
College of Chemistry
Nankai University
Tianjin 300071, P. R. China
E-mail: yuliu@nankai.edu.cn

B. Qiao
College of Chemistry
Beijing Normal University
Beijing 100875, P. R. China

The ORCID identification number(s) for the author(s) of this article can be found under https://doi.org/10.1002/adom.202503320

DOI: 10.1002/adom.202503320

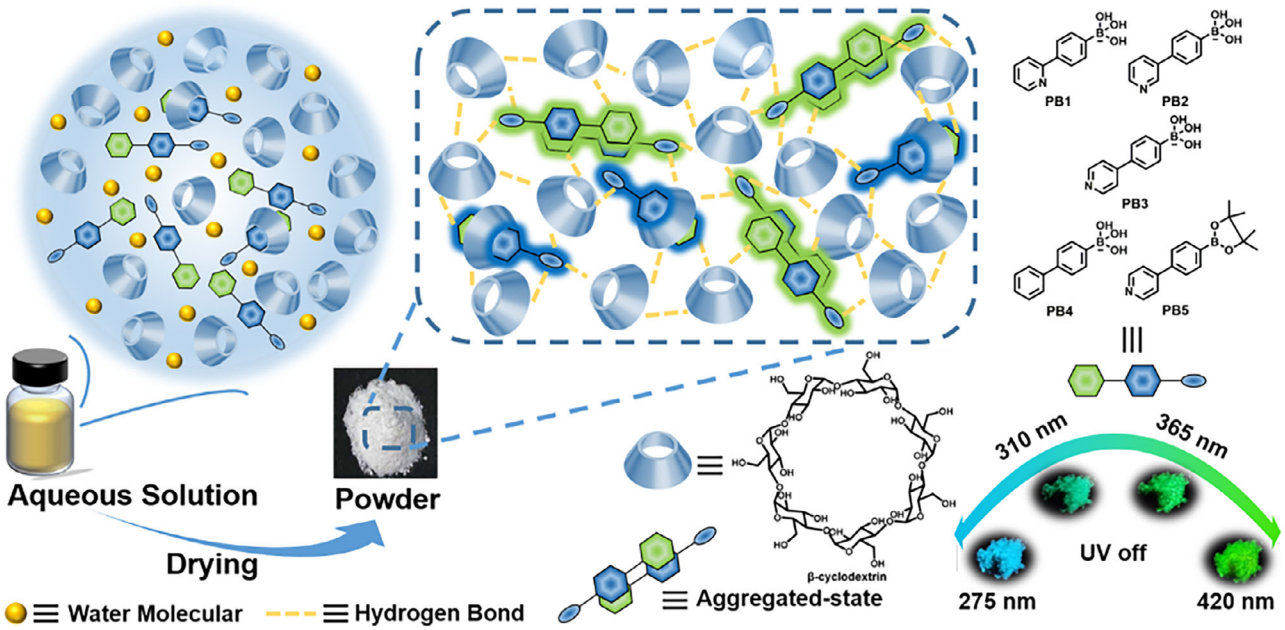

Scheme 1. Schematic representation of the preparation procedure for β-cyclodextrin-based self-assembled systems and single-phosphor multichromatic afterglow, with the molecular structures of phosphors and the host matrix.

phosphors. Consequently, the self-assembled system can generate yellow-green phosphorescence even under visible light (white light) excitation. Furthermore, the single phosphor achieves wide-range afterglow modulation spanning blue, cyan and green to yellow-green when supported by the ideal host matrix β-cyclodextrin. This has significant potential for use in multicolor dynamic displays and information storage.

2. Results and Discussion

Five different boronic acid-based compounds were chosen as luminescent guests: 4-(pyridin-2-yl)phenylboronic acid (PB1), (4-(pyridin-3-yl)phenyl)boronic acid (PB2), (4-(pyridin-4-yl)phenyl)boronic acid (PB3), 4-biphenylboronic acid (PB4) and 4-(4-pyridinyl)phenylboronic acid pinacol ester (PB5) (Figure S1, Supporting Information). The pyridine group's lone pair of electrons can facilitate potential n-π^* transitions for spin-orbit coupling. To increase the solubility of the guest molecules in water and prevent precipitation from affecting the luminescence of the system, an appropriate amount of potassium carbonate was added to the system. To obtain stimuli-responsive, environmentally friendly, highly efficient, room-temperature phosphorescent materials, we used β-cyclodextrin as the matrix. This is a macrocyclic molecule with a rigid structure and contains a unique cavity structure, as well as abundant intramolecular and intermolecular hydrogen bonding. This provides a rigid framework that inhibits the non-radiative decay of triple excitations.

2.1. Photophysical Properties

Following the doping of guest molecules into β-cyclodextrin to form powders, both the resulting PB3@β-CD and PB5@β-CD powders exhibited bright and intense phosphorescence, with afterglow persisting for several seconds (Figures S2 and S3, Supporting Information). In this study, the sample was exposed to uniform illumination for a duration of 10 s prior to the acquisition of the afterglow images. The subsequent section presents afterglow photographs of the supramolecular self-assembled system PB3@β-CD under varying durations of light exposure (Figure S4, Supporting Information). Subsequently, we recycled the supramolecular self-assembly system PB3@β-CD to obtain afterglow images. The results demonstrate that the system retains excellent afterglow performance even after recovery (Figure S5, Supporting Information). It is evident that the cluster-induced luminescence of the polysaccharides has a significant impact on the emission properties of the pristine β-CD. While the emission from the pristine β-CD is weak, it is negligible when compared to the doped system (Figure S6, Supporting Information). Identically, phosphorescence emission peaks are exhibited in the phosphorescence spectra measured from PB1@β-CD, PB2@β-CD, PB3@β-CD PB4@β-CD and PB5@β-CD powder tests (Figure S7, Supporting Information). In particular, PB3@β-CD exhibited the most favourable excitation wavelength-dependent property. It was demonstrated that when the excitation wavelength was altered from 254 to 400 nm, PB3@β-CD exhibited phosphorescence emission spectra that were dependent on the excitation wavelength. In contrast to other observations, the two emissions with peaks at 465 and 520 nm in the phosphorescence spectrum are comparable in intensity. Furthermore, two distinct emission regions with peaks at 465 and 520 nm can be identified in the excitation pattern of phosphorescence emission (**Figure 1a**). It is demonstrated that altering the excitation wavelength from 254 to 400 nm (Figures 1b; S8, Supporting Information) results in a distinct redshift color shift, from sky blue, cyan and yellowish-green, to green. In addition, there is a shift

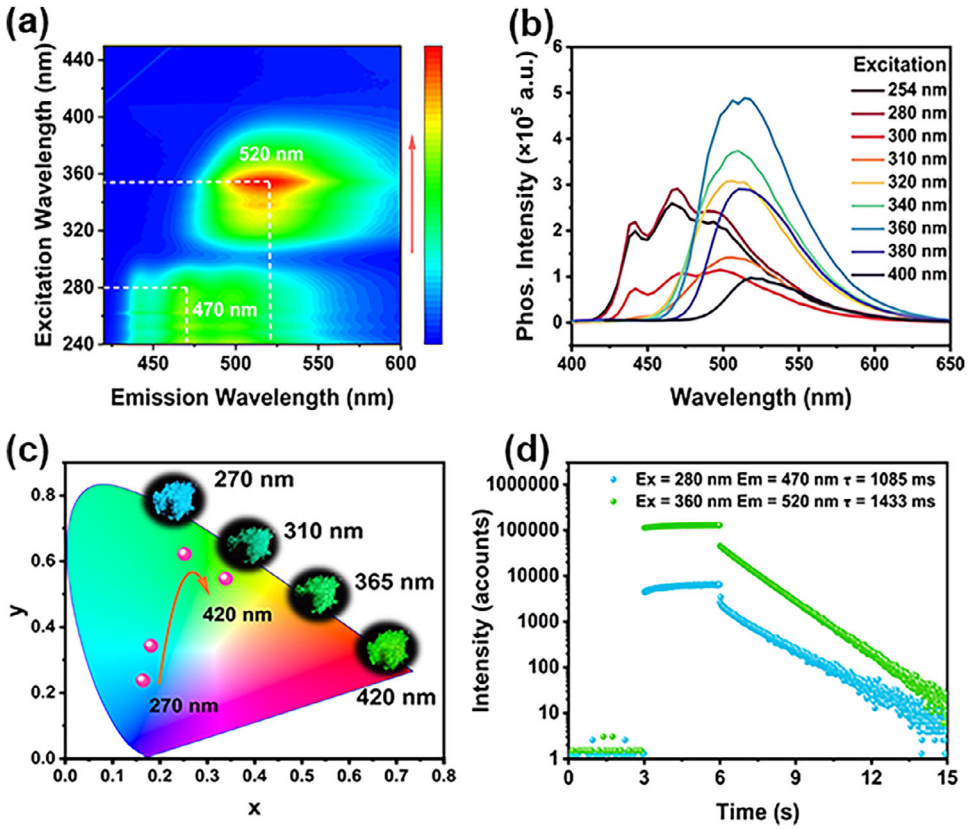

Figure 1. a) Excitation-phosphorescence mapping of PB3@β-CD. b) Phosphorescence spectra of PB3@β-CD excited by different wavelengths. c) CIE chromaticity coordinates of PB3@β-CD at various excitation wavelengths. Inset: afterglow images of the PB3@β-CD at various excitation wavelengths. d) Lifetime profiles for the phosphorescence of PB3@β-CD; doping concentration: 10 mol%.

of the emission maximum, from 465 to 520 nm, and a concomitant alteration of the afterglow colors in the Commission International de I'Eclairage (CIE) coordinate chart (Figure 1c). In contrast, the guest molecule PB1 exhibits excitation-dependent features subsequent to forming an assembly with β-CD. However, when the excitation wavelength is varied from 254 to 400 nm, emission peaks are observed only within the wavelength range of 475 to 500 nm, exhibiting a redshift phenomenon from cyan to light green (Figure S9a,b, Supporting Information). With regard to the pyridine group, the resulting guest molecule, PB2, exhibits diminished excitation-dependent characteristics following the formation of an assembly with β-CD when the N atom is in the 3rd position (Figure S10a,b, Supporting Information). The intensity of the phosphorescence emission of the assembly PB2@β-CD gradually becomes weaker with the change of excitation wavelength, and shows weak emission at 340 nm excitation. Specifically, the emission intensity of the supramolecular self-assemblies PB2@β-CD upon 260 nm excitation is approximately eight times that observed under 360 nm excitation. Furthermore, the phosphorescence emission lifetime of the self-assemblies under 360 nm excitation is only about half that observed under 260 nm excitation. The guest molecule PB4, which has been obtained by substituting the pyridine group in the guest molecule PB3 with a phenyl group, also exhibits weaker excitation-dependent features under the same conditions (Figure S11a,b, Supporting Information).

In a similar manner, the emission intensity of the supramolecular self-assemblies PB4@β-CD upon 360 nm excitation is negligible in comparison to that under 260 nm excitation; the phosphorescence emission lifetime of the self-assemblies under 360 nm excitation is also approximately half that under 260 nm excitation. The guest molecule PB5, obtained by esterifying the guest molecule PB3 and forming an assembly with β-CD under the same conditions, also exhibits a phosphorescence emission spectrum that is dependent on the excitation wavelength when the excitation wavelength is changed from 254 to 380 nm. Furthermore, the phosphorescence spectra of PB5 are very similar to the phosphorescence spectra of PB3@β-CD (Figure S12a,b, Supporting Information). In contrast to other guests, PB5 exhibits the same phenomenon in the β-CD matrix as the supramolecular self-assemblies PB3@β-CD: at a 10 mol% doping concentration, the phosphorescence emission intensity of the supramolecular self-assemblies PB5@β-CD upon excitation at 360 nm is comparable to that upon excitation at 260 nm. The phosphorescence emission lifetime of the self-assemblies upon excitation at 360 nm is also quite similar to that upon excitation at 260 nm. A comparative analysis of the lifetimes and emission centers of the two self-assembled systems reveals only slight disparities. Concurrently, within this series of boronic acid derivatives, PB3 and PB5 demonstrate a notably superior excitation-dependent response. Simultaneously, the phosphorescence emission lifetimes of PB1@β-CD, PB2@β-CD, PB3@β-CD, PB4@β-CD and

PB5@β-CD powders upon excitation at 260 nm were measured to be 1307, 1371, 1085, 2511 and 1334 ms, respectively, while their phosphorescence emission lifetimes upon excitation at 360 nm were measured to be 1456, 788, 1433, 1159 and 1084 ms, respectively (Figures 1d; S9c, S10c, S11c and S12c, Supporting Information). The photoluminescence quantum yield of the PB3@β-CD powders was measured to be 34.89%, while the phosphorescence quantum yield was 24.91%. However, the five compounds in question do not exhibit afterglow under UV excitation (Figures S13 and S14, Supporting Information). This phenomenon could be attributed to phosphorescence quenching resulting from aggregation. It is evident that molecular motion is constrained in the presence of the β-cyclodextrin framework, which stabilizes the triplet excited state and facilitates radioactive decay.

Chromophores exist in different isolated and aggregated states in the host matrix, and the energy levels of the excited states change, resulting in special optical properties such as concentration dependence and excitation wavelength dependence. For PB3@β-CD, the phosphorescence emission intensity (Figure S15a, Supporting Information) and lifetime (τ) of the self-assembled system upon excitation at 260 nm (Figure S16b, Supporting Information) reached a maximum and stabilized within the host-guest concentration range of 1–15%. Within this range, 10 mol% corresponds to the intermediate value. It has been demonstrated that lower host-guest concentrations result in insufficient light absorption, while excessively high concentrations cause decreased phosphorescence emission intensity due to over-aggregation. Furthermore, the I_{512}/I_{468} of PB3@β-CD increased rapidly as the host-guest concentrations increased from 0.1 to 0.5%, however, as the host-guest concentrations further increased, the phosphorescence emission intensity and lifetime remained basically unchanged (Figure S16a, Supporting Information). Moreover, the emission intensity of the self-assembled system under 360 nm excitation is comparable to that under 260 nm excitation. As illustrated in Figure S17 (Supporting Information), the phosphorescence emission intensity value of PB3 monomers in the β-CD matrix at a 10 mol% concentration is 669 279, whereas that of PB3 aggregates in the β-CD matrix is 670 376. Consequently, 10 mol% was selected as the optimal host-guest concentration for investigating the excitation-dependent properties of the system. In order to provide clear evidence of the coexistence of isolated and aggregated states of PB3 within the β-CD matrix, phosphorescence spectra were recorded at 260 and 360 nm after excitation of PB3@β-CD supramolecular self-assemblies under ambient conditions, at both low (0.1 mol%) and high (20 mol%) host-guest doping contents (Figure S18a,b, Supporting Information). In PB3@β-CD supramolecular self-assemblies with low host-guest dopant content, PB3 predominantly exists in an isolated state; whereas in PB3@β-CD supramolecular self-assemblies with high host-guest dopant content, PB3 primarily exists in an aggregated state. The assembly of PB3@β-CD was obtained by subjecting an aqueous mixture of PB3 and β-CD to sonication, heating and vacuum drying, with potassium carbonate-assisted dissolution. For the purpose of comparison, four distinct co-solvent-assisted PB3@β-CD assemblies have been prepared, with phosphorescence emission spectra and lifetime decay curves appended to the supporting information (Figures S19–S21, Supporting Information). As demonstrated in Figures S19b and S22a (Supporting Information), in the presence of KOH, the guest PB3 does not exhibit phosphorescence dominated by the monomer emission even at a guest-to-host β-cyclodextrin molar ratio of 0.1 mol%. As demonstrated in Figures S19c, and S22b (Supporting Information), in the presence of Na_2CO_3, even at a 20 mol% guest-to-host molar ratio of PB3 to β-cyclodextrin, the guest PB3 fails to exhibit phosphorescence emission dominated by aggregate emission. As demonstrated in Figures S19d, and S22c (Supporting Information), when the guest-to-host molar ratio was calibrated to 20 mol% in the presence of NaOH, the guest PB3 exhibited phosphorescence emission dominated by aggregated states. However, in comparison to the supramolecular self-assembled system in the presence of potassium carbonate, it exhibited a significantly weaker excitation wavelength dependence. The results indicate that potassium carbonate not only acts as a solubility aid but also modulates the aggregation state of the guest within the matrix, thereby exerting an influence on the excitation-dependent properties of the system.

2.2. Mechanism Analysis for the Excitation-Dependence and Single-Phosphor Multichromatic Emission

The universality of the excitation-dependent feature of self-assembly is the subject of further discussion. The experimental results indicate that self-assembled systems containing guest molecules PB1 and PB5 also exhibit excitation-dependent characteristics similar to those of PB3@β-CD. Conversely, self-assembled systems comprising guest molecules of PB2 and PB4 do not manifest such phenomena. Neither PB2@β-CD nor PB4@β-CD exhibited phosphorescence peaks of any noticeable intensity upon excitation at 360 nm. This phenomenon may be attributed to the positioning of the N atom within the molecule. In considering the guest molecule PB2, the 2D ROESY (rotating-frame overhauser effect spectroscopy) spectra of PB2 and the host β-cyclodextrin (Figure S38, Supporting Information) demonstrate the guest molecule in a head-to-tail stacked mode. However, this is not as clearly evident as the head-to-tail stacked mode of the guest molecule PB3 (Figure S39, Supporting Information). As demonstrated in Figures 1b and S10b (Supporting Information), this phenomenon is consistent with the spectral properties of the system. In particular, the emission intensity and lifetime of relatively difficult-to-aggregate guests are weaker under 360 nm excitation. An investigation was conducted into the PB3 assembly in the presence of diverse host molecules. The results obtained from this investigation were analogous to those previously observed in conjunction with β-cyclodextrin. The phosphorescence emission intensity and lifetime exhibited by PB3@γ-CD, PB3@PVP (polyvinylpyrrolidone) and PB3@PVA (poly(vinyl alcohol)) are presented in this study (Figures S23, S26 and S27, Supporting Information) were comparable to those of PB3@β-CD, whereas PB3@α-CD (α-cyclodextrin), PB3@HP-β-CD (hydroxypropyl β-cyclodextrin) and PB3@PAM (Polyacrylamide) (Figures S24, S25 and S28, Supporting Information) demonstrated relatively weaker phosphorescence emission intensity and lifetime. Potential explanations for this phenomenon may be attributed to the degree of matching between the hydrophobic cavity dimensions and the guest molecules, as well as the significant role of regular hydrogen bonding

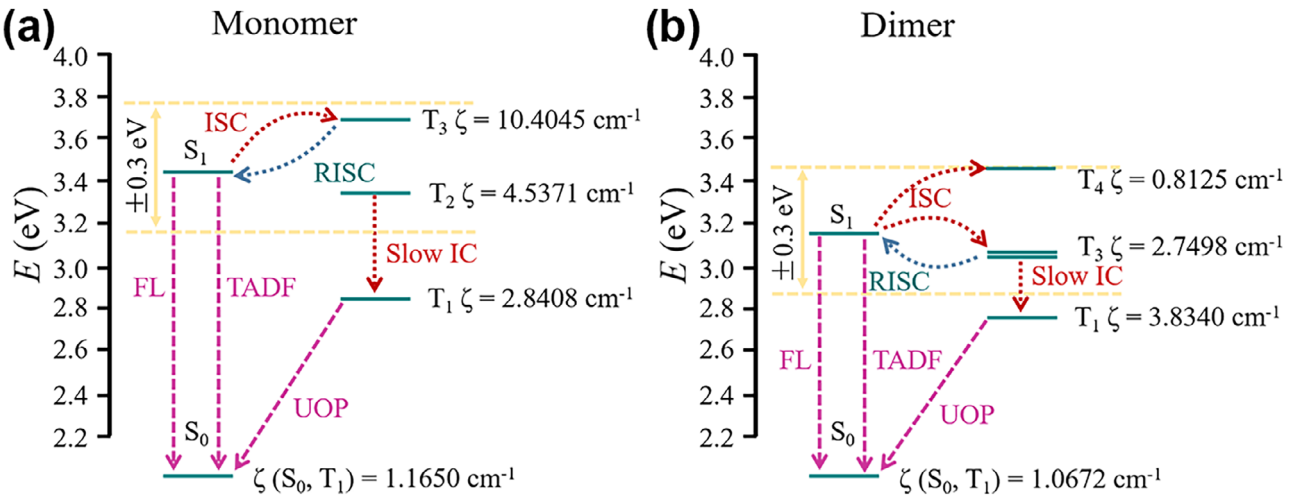

Figure 2. a,b) Diagram of the calculated energy levels, the possible ISC channels with the ξ of the PB3 monomer and the PB3 dimer, respectively.

interactions in phosphorescence excitation-dependent characteristics. Among them, PB3@PVP demonstrates adequate phosphorescence emission intensity and lifetime, which can be ascribed to the pyrrolidone ring structure in the polymer PVP in the solid-state matrix, furnishing a distinctive rigid foundation for its excitation-dependent characteristics (Figure S26, Supporting Information). The γ-cyclodextrin with a larger cavity was able to form an inclusion compound with the guest molecule PB3 and exhibited excitation-dependent features, but the lifetime of the assemblies was slightly inferior compared to that of PB3@β-CD. It has been demonstrated that materials prepared using PB3 and polyvinyl alcohol (PB3@PVA) exhibit similar properties to those prepared with β-cyclodextrin (β-CD). However, PB3@PVA demonstrates a narrower excitation range (254–340 nm) and emission wavelength shift (460–500 nm) (Figure S27, Supporting Information). In contrast, PB3@β-CD exhibits a broader excitation range (254–400 nm) and emission wavelength shift (465–520 nm) (Figure 1). In comparison with β-cyclodextrin, the assemblies formed by α-cyclodextrin with a smaller cavity and PB3 did not exhibit excitation-dependent features. This is primarily attributed to the inability of α-cyclodextrin with a smaller cavity to form an inclusion compound with the guest molecule PB3. The assemblies formed by PB3 with HP-β-CD did not exhibit excitation-dependent features either, which can be attributed to the regular rigid structure of β-cyclodextrin. Assemblies of β-cyclodextrin displayed excellent luminescence properties and excitation-dependent characteristics. In contrast, following the replacement of the substrate with polymer PAM, PB3@PAM did not exhibit excitation wavelength-dependent phosphorescence emission spectra when the excitation wavelength was varied from 254 to 360 nm. (Figure S28, Supporting Information). In comparison, the assemblies formed by the reference guest 4-(pyridin-4-yl)benzonitrile (P1) (Figure S1, Supporting Information) with β-cyclodextrin exhibit only short lifetimes at 475 nm (Figure S29, Supporting Information) and show almost no excitation-dependent features. This is due to the enhancement of the electron-withdrawing ability of the substituents of the guest molecule. In comparison with the guest molecule P1, the carboxyl-substituted reference guest 4-pyridin-4-yl-benzoic acid (P2), which possesses relatively weak electron-withdrawing ability, and the reference guest 4-phenylpyridine (P3), which lacks substituent groups, do not manifest excitation-dependent features. However, both exhibit satisfactory lifetimes of ≈470 nm (Figures S30 and S31, Supporting Information). Conversely, the enhanced electron-donating capacity of the para-substituents in the phenylpyridine derivatives (4-(pyridin-4-yl)phenol (P4) and (4-(pyridin-4-yl)aniline (P5)) results in the excitation-dependent phosphorescence spectra of the assemblies P4@β-CD and P5@β-CD not displaying additional emission regions as the excitation wavelengths vary from 260 to 360 nm (Figures S32 and S33, Supporting Information). In order to investigate the nature of the delayed emission in this system, the temperature-dependent phosphorescence spectra were analyzed. Excitation at 260 nm results in a gradual enhancement of the delayed emission band at 418 nm and a gradual weakening of the delayed emission band at 466 nm as the temperature is increased from 233 to 373 K (Figure S34a, Supporting Information). This suggests that the emission band at 418 nm possesses a delayed fluorescence (DF) property, whereas the emission band at 465 nm exhibits ultralong organic phosphorescence (UOP) properties. It has been demonstrated that, at temperatures in excess of 313 K, the intensity of the DF band surpasses that of the UOP band. In a similar manner, the phosphorescence spectrum, when subjected to excitation at 360 nm, undergoes a shift in emission from the predominant 520 nm to the 440 nm when the temperature is elevated from 333 to 433 K. (Figure S34b, Supporting Information). In contrast to the behaviour observed under 260 nm excitation, the intensity of the thermally activated delayed fluorescence (TADF) band exceeds that of the UOP band when the temperature is greater than 413 K and the excitation wavelength is 360 nm. This finding suggests that the TADF process in the aggregated state requires a higher activation temperature than in the isolated state, resulting in the layered dual-mode delayed emission observed in the PB3@β-CD system. The influence of temperature on the delayed emission spectrum of the assembly can be more clearly observed through its CIE chromaticity diagram (Figures S34c and S34d, Supporting Information). In order to provide further confirmation of the aggregation pattern

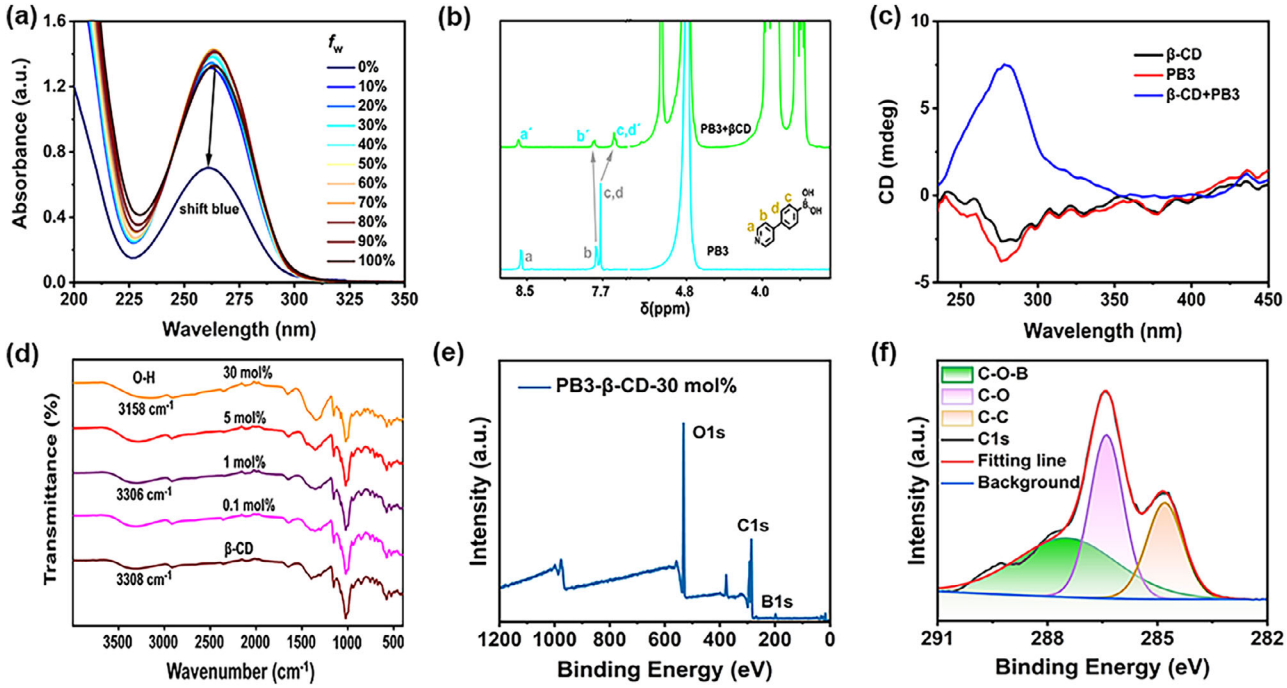

Figure 3. a) Absorption spectra of PB3 solutions in various ethanol/H_2O mixtures (10^{-4} M). b) ^{1}H NMR (400 MHz, D_2O, 298 K) spectra of PB3 (3 mM) and PB3+β-CD (3 mM: 30 mM). c) Circular dichroism spectra of PB3@β-CD. d) FT-IR spectra of PB3@β-CD with different doping ratio and β-CD. e) XPS spectra of PB3@β-CD-10 mol%. f) High-resolution XPS for C1s of PB3@β-CD-10 mol%.

of PB3 molecules in self-assemblies, the absorption spectra of PB3 solutions in ethanol/H_2O mixtures with different H_2O ratios were studied. PB3 demonstrates high solubility in ethanol, while H_2O, acting as a non-solvent, brings monomers closer together, eventually forming aggregated species. As demonstrated in Figure 3a, the blue-shifted absorption band that emerges with increasing water fraction (f_w) signifies that PB3 exhibits a propensity to form H-aggregates rather than J-aggregates in water. In order to achieve a more profound comprehension of the afterglow phenomenon in this system, theoretical calculations were conducted on the basis of density functional theory (Tables S1–S3, Supporting Information). The phosphorescence emission spectra of PB3@β-CD supramolecular self-assemblies at low concentrations are indicative of PB3 primarily existing in an isolated state within the β-CD matrix, whereas at high concentrations it predominantly exists in an aggregated state (Figure S18, Supporting Information). Furthermore, analysis of the 2D NMR spectrum (Figure S40, Supporting Information) reveals a distinct interaction between the proton on the pyridine group of one PB3 guest molecule and the proton on the phenyl group of another PB3 guest molecule. This finding suggests that the guest molecules exist in a head-to-tail stacked aggregate mode. Therefore, theoretical calculations were performed for the monomer and dimer of the guest molecule using density functional theory. As shown in **Figure** 2a, based on the large spin-orbit coupling matrix element (SOCME, 10.4045 cm^{-1}) and relatively small singlet-triplet energy gap (ΔE_{ST}) (0.267 eV), the potential $S_1 \rightarrow T_n$ pathway for isolated PB2 was calculated as $S_1 \rightarrow T_3$, indicating that T_3 can function as a conduit to facilitate the ISC/ RISC process. Furthermore, a relatively large energy gap (ΔE_g = 0.4927 eV) was identified between T_1 and T_2, suggesting that the internal conversion (IC) process may be relatively slow. Consequently, due to the slow relaxation to the T_1 excited state, the conversion of long-lived triplet excitons in the T_2 and T_3 states to the S_1 state is promoted, leading to the emergence of TADF phenomena in the PB3@β-CD system. For the PB3 dimer representing the H aggregate state (Figure 2b), potential ISC pathways exist from S_1 to T_3 and T_4. These are characterized by large SOC constant (ξ) values (2.7498 and 0.8125 cm^{-1}) and small ΔE_{ST} values (0.0922 and 0.2962 eV). This indicates that RISC activation in the H-aggregate state requires higher temperatures than in the isolated state. It is hypothesized that PB1, PB2, and PB4 may possess RISC channels, with their ΔE_{ST} values (PB1: 0.0754 eV, PB2: 0.0136 eV, PB4: 0.0694 eV) all being smaller than that of PB3 (Tables S4–S6 and Figure S53, Supporting Information). This suggests that PB1@β-CD, PB2@β-CD, and PB4@β-CD will also exhibit delayed fluorescence emission.

In order to provide further elucidation on the assembling mode, a range of analytical techniques were employed, including FT-IR, XPS, NMR, and circular dichroism, in order to facilitate the analysis of the various interactions within the self-assembling systems. The ^{1}H NMR spectrum indicates that both the pyridine and phenyl protons exhibit a certain degree of chemical shift in the presence of β-cyclodextrin, suggesting the formation of an inclusion complex (Figure 3b). In comparison with methylated β-cyclodextrin, it can be observed that in the presence of β-cyclodextrin, the proton on the phenyl group exhibits only a significant upfield shift without noticeable cleavage. This finding implies that there is a significant hydrogen-bonding interaction between the hydroxyl group on the β-cyclodextrin and the hydroxyl group on the PB3 (Figure S35, Supporting Information). This phenomenon also provides an explanation for the

excellent luminescence behaviour of the assembly and its excitation dependence. In the presence of γ-cyclodextrin, which possesses a more substantial cavity, both the pyridyl and phenyl protons on PB3 exhibited a shift to a higher field. This observation indicates the presence of interactions between the γ-cyclodextrin cavity and the pyridyl and phenyl groups of the guest molecule PB3. In the case of α-cyclodextrin with a smaller cavity, only the pyridyl proton on PB3 moves to the lower field position. This demonstrates that only the pyridine group of the guest molecule PB3 interacts with α-cyclodextrin. The failure of α-cyclodextrin to encapsulate at the phenyl position of the guest molecule PB3 resulted in a significant attenuation of the luminescence behaviour of the assemblies. In contrast with the interaction with β-cyclodextrin, the phenyl protons on PB3 underwent a high-field shift and also demonstrated significant cleavage in the presence of hydroxypropyl β-cyclodextrin. It is evident that the homogeneity of the hydroxyl groups located at the two orifice ends of the cyclodextrin cavity exerts a substantial influence on the exceptional luminescence behaviour and excitation-dependent properties of the assemblies. This finding was corroborated by 2D nuclear magnetic resonance analysis, which yielded consistent results. Specifically, the ROESY (rotating-frame overhauser effect spectroscopy) spectra of PB1, PB2, and PB3 exhibited strong rotating frame nuclear Overhauser effect signals with β-cyclodextrin (Figures S36, S37 and S39, Supporting Information). As demonstrated in Figure S39 (Supporting Information), the proton peak on the phenyl group of the guest molecule PB3 exhibits a strong interaction with the proton peaks at positions 5 and 6 on β-cyclodextrin. As demonstrated in Figure S40 (Supporting Information), the phenyl proton peak of the aggregated PB3 guest molecule interacts with the pyridine proton peak of another PB3 guest molecule. Consequently, in Scheme 1, the phenyl group is located at the small mouth end of β-cyclodextrin during host-guest association; in the aggregated state, guest molecules stack in a head-to-tail configuration. In order to investigate the mechanism of efficient multicolor RTP emission in the PB3@β-CD system, the host-guest interaction between PB3 and β-CD was analyzed using UV-visible titration experiments. As demonstrated in Figure S43 (Supporting Information), the absorption undergoes a change in response to the incremental addition of β-CD, attributable to the binding between the PB3 monomer and β-CD. The binding constant (*Ks*) of the PB3@β-CD system has been determined to be 175.70 M^{-1}. Concurrently, the binding constants for PB1@β-CD, PB2@β-CD and PB4@β-CD were measured at 109.57, 505.83 and 1295.37 M^{-1}, respectively (Figures S41, S42, and S44, Supporting Information). In accordance with the aforementioned findings, the binding constants for PB3@α-CD and PB3@γ-CD were measured at 76.18 and 111.80 M^{-1}, respectively (Figures S45 and S46, Supporting Information).

In addition, given the chiral nature of the cavity of β-cyclodextrin, an option for determining whether a guest molecule is recognized is to seek strong circular dichroism signals arising from spatial chiral transfer. It has been demonstrated that both β-cyclodextrin and PB3 exhibit relatively weak circular dichroism signals when analyzed individually. However, following the formation of the PB3@β-CD assembly, the host and guest molecules present mirror-image signals (Figure 3c). Within the 240–350 nm range, an impressive Cotton effect is observed, with signal positions correlating with absorption peaks (Figure S47, Supporting Information). This indicates the occurrence of host-guest encapsulation between PB3 and β-cyclodextrin within the self-assembled system. The rigidity of the environment provided by hydrogen bonding is widely utilized in the construction of RTP materials, while the hydroxyl structure of β-CD offers a prerequisite for hydrogen bond formation. Figure 3d displays the FT-IR spectra of PB3@β-CD and β-CD with varying doping ratios. As the PB3 doping ratio increases, the characteristic O—H absorption peak at 3308 cm^{-1} gradually broadens and shifts, indicating hydrogen bonding interactions between PB3 and β-CD. The hydrogen bond interactions in question suppress the vibration of the luminophore, thereby enhancing the survival of triplet excitons. As demonstrated in Figure 3e, the doped system PB3@β-CD-30 mol% contains C, O, and B elements. As demonstrated in Figure 3f, a three-peak fitting is observed in the high-resolution spectrum of the C1s curve, thereby confirming the presence of C—O—B (287.8 eV), C—O (286.3 eV), and C—C (284.1 eV) bonds within the self-assembled system. It has been demonstrated that, upon attaining a concentration of 0.1 M, the PB3@β-CD system precipitates crystals following a process of heating and cooling. The crystals and solution were then subjected to separation and drying in separate processes. The phosphorescence spectra obtained from the dried crystals under 260 nm excitation are analogous to those obtained from the dried solution powder, and their lifetimes are also similar (**Figures** 4a; S48, Supporting Information). However, the emission from the dried crystals under 260 nm excitation is more blue than that from the powder under 260 nm excitation, as clearly demonstrated in the CIE diagram (Figures 4b; S49, Supporting Information). In the absence of 360 nm excitation, the powder emits yellow-green light at 520 nm. It is evident that guest PB3 exists solely in an isolated state within the cavity of the β-cyclodextrin crystal, whereas in the powder, guest PB3 can coexist in both isolated and aggregated states within the system. The formation of the PB3@β-CD self-assembled system enables tunable emission wavelengths to achieve adjustable multicolor afterglow and broadens the absorption wavelength range. The results obtained from this study indicate that PB3@β-CD exhibits absorption and phosphorescence wavelengths (at room temperature) spanning 250–430 and 440–550 nm, respectively. Furthermore, the excitation spectrum of phosphorescence emission reveals that the guest molecules can be excited by light in a wide wavelength range of 250–430 nm, demonstrating that they can be activated by non-UV light. It is noteworthy that PB3@β-CD self-assembled powders continue to exhibit yellow-green afterglow at excitation wavelengths in excess of 400 nm, a range that partially overlaps with the emission spectrum of white light-emitting diodes (LEDs). Consequently, PB3@β-CD self-assembled powders can be excited through the utilization of conventional lighting equipment and flashlights. The experimental results obtained in this study provide further evidence that when exposed to white light, PB3@β-CD displays a vivid yellow-green afterglow with a duration of approximately three seconds (Figure 4c). As the delay spectrum is excitation-dependent, the afterglow color of the crystal powder under visible light illumination closely resembles that produced by 365 nm UV excitation, facilitating practical applications. In comparison with UV light, white light has been demonstrated to offer

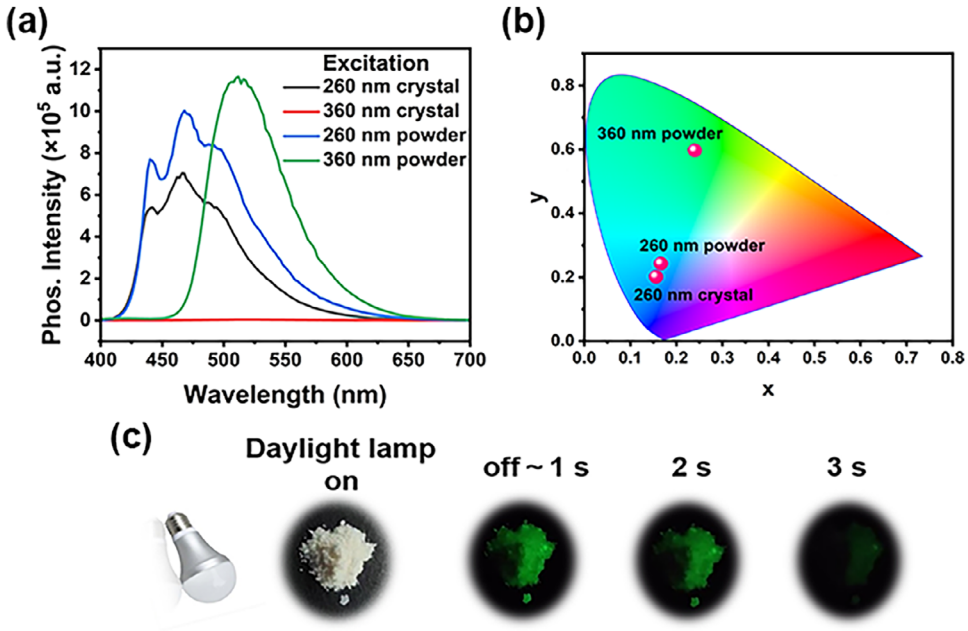

Figure 4. a) Phosphorescence spectra of PB3@β-CD in powder and crystal states under excitation at 260 nm and 360 nm. b) CIE chromaticity coordinates of PB3@β-CD in powder and crystal states under excitation wavelengths of 260 and 360 nm. c) Afterglow photographs of PB3@β-CD excited at white-light. Doping concentration: 10 mol%.

superior biocompatibility, thereby enabling white-light-excited phosphorescent materials to deliver unique advantages in the domain of biological tissue imaging. It is evident from the significant overlap between the phosphorescence spectrum of PB3@β-CD and the absorption spectrum of Sulforhodamine 101 (SR101) that there has been efficient energy transfer from the triplet to the singlet state, as illustrated in Figure S50a (Supporting Information). Subsequently, the dye molecule SR101 was loaded as an energy-transfer acceptor into the supramolecular self-assembled system PB3@β-CD (Figure S50b, Supporting Information). It was surprising that, despite the fact that pure white phosphorescence was not obtained from the dye-loaded system PB3@β-CD/SR101 (n_{PB3}: n_{SR101} = 50:1), near-white phosphorescence was achieved, which enriches the multicolor luminescence behaviour of the system.

2.3. Application for Information Encryption and Anti-Counterfeiting

In light of the fact that polyvinyl alcohol (PVA) boasts excellent flexibility, processability, and superior film-forming capability, in conjunction with the outstanding excitation-dependent properties exhibited by the supramolecular self-assembly system PB3@β-CD, it was decided to incorporate PVA into the PB3@β-CD self-assembly system in order to evaluate the feasibility of PB3@β-CD/PVA. It is evident from the excitation wavelength ranges and emission wavelength shifts (Figures S27 and S51, Supporting Information) exhibited by the supramolecular self-assembly systems PB3@PVA and PB3@β-CD/PVA that the presence of β-CD has a slightly enhancing effect on the properties of PB3@PVA. Conversely, the presence of PVA endows the PB3@β-CD system with both flexibility and film-forming capability. For the PB3@β-CD/PVA system, the phosphorescence emission intensity of the self-assembled structure measured under 260 nm excitation (Figure S51a, Supporting Information) reached its maximum at a host-guest concentration of 2%. In a similar manner, the phosphorescence emission intensity of the self-assembled structure measured under 360 nm excitation (Figure S51b, Supporting Information) also peaked at a host-guest concentration of 2%. It can be observed that the 2 wt.%-PB3@β-CD/PVA system exhibits superior emission intensity and extended lifetime (Figure S51c,d, Supporting Information), indicating that the synergistic assembly of PB3@β-CD with PVA can also achieve excellent phosphorescent properties (Figure S51e,f, Supporting Information). In conclusion, the PB3@β-CD/PVA system's inherent flexibility, customisability and ease of preparation were successfully exploited to produce 3D patterns of letters, snowflakes and numbers. (**Figures** 5a,b; S52, Supporting Information). These objects exhibit two distinctive characteristics. First, they demonstrate persistent phosphorescence emission. Second, they exhibit excitation-dependent multicolor afterglow phenomena. As demonstrated in Figure 5c, filter paper is immersed in the PB3@β-CD solution and subsequently dried, resulting in the formation of the Chinese character "开". This pattern demonstrates a specific degree of temperature-dependent afterglow when exposed to excitation at 275 and 365 nm, with the afterglow of the pattern at 365 nm excitation remaining discernible to the naked eye at 162 °C.

As demonstrated in Figure 5d, the solution is injected into the groove of a polytetrafluoroethylene mold, then dried, and the PB3@β-CD/PVA system can be fabricated into a high-resolution quick response (QR) code. It is evident that the QR code pattern exhibited following UV irradiation can be scanned and

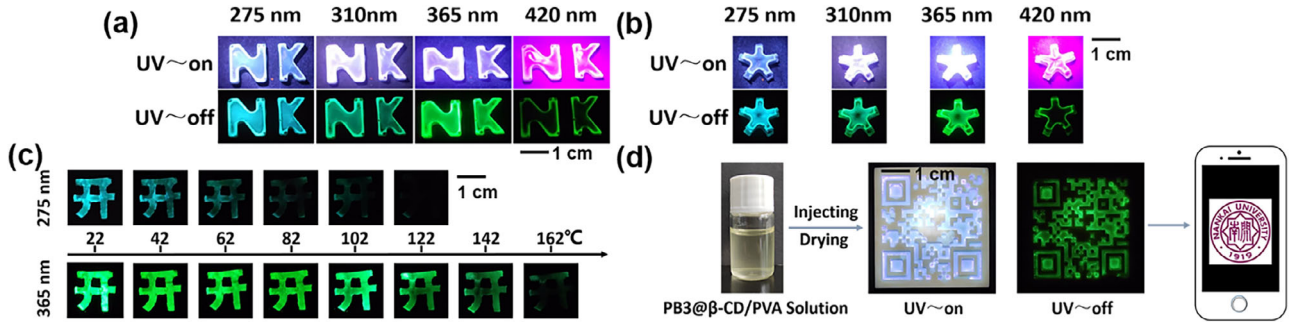

Figure 5. a,b) Photographs of 3D patterns prepared using PB3@β-CD/PVA under ambient conditions with UV lamps at 275, 310, 365 and 420 nm on and off. c) Photographs of the afterglow of Chinese character "开" prepared by the PB3@β-CD solution on excitation at 275 and 365 nm. d) Schematic diagram of the QR code pattern prepared using PB3@β-CD/PVA solution, along with the afterglow image excited by 365 nm. Copyright Nankai University. The time interval between illumination cessation and image recording is 0.5 s.

recognized by a mobile phone due to its satisfactory afterglow quantum yield and lifetime.

3. Conclusion

In summary, a supramolecular monophosphor multicolor room-temperature phosphorescence (RTP) material was successfully constructed using biomass β-CD. The hydrogen bonds and host-guest encapsulation exhibited by β-CD were found to be significant in the suppression of non-radiative transitions, thereby enabling the phenylboronic acid derivatives to exhibit multicolor afterglow upon excitation at different wavelengths. The PB3@β-CD system exhibits a broad excitation range (240–420 nm) and undergoes color transitions (blue to yellow-green). Its cost-effectiveness, eco-friendliness, and non-toxicity are key factors in the advancement of sustainable RTP materials, which hold great promise for applications in the domains of information storage, displays, and encryption.

4. Experimental Section

Preparation of Supramolecular Assembly PB3@β-CD: An aqueous solution (5 mL) of β-cyclodextrin (0.2 mmol) and potassium carbonate (1 mmol) was thoroughly mixed with (4-(pyridin-4-yl)phenyl)boronic acid (0.02 mmol), dissolved completely and baked at 80 °C under vacuum for 8 h to obtain self-assembling powder. It was then dried in a vacuum oven at 100 °C for 5 h to remove residual moisture for subsequent testing.

Preparation Process of the PB3@β-CD/PVA System: Aqueous solutions of PB3 (1.99 mg, 0.01 mmol), β-cyclodextrin (113.5 mg, 0.1 mmol), and K_2CO_3 (69 mg, 0.5 mmol) (2 mL) were heated and stirred until dissolution. A 10% polyvinyl alcohol aqueous solution (1 mL) was then added, and the mixture was stirred for 1 h. The mixture was baked under vacuum at 60 °C for 8 h to obtain a self-assembled film. Subsequently, the film was dried in a vacuum oven at 90 °C for 5 h to remove residual moisture for subsequent testing.

Preparation of the Patterns: Aqueous solutions of PB3 (1.99 mg, 0.01 mmol), β-cyclodextrin (113.5 mg, 0.1 mmol), and K_2CO_3 (69 mg, 0.5 mmol) (2 mL) were heated and stirred until dissolution. A 10% polyvinyl alcohol aqueous solution (1 mL) was then added, and the mixture was stirred for 1 h. Subsequently, a corresponding volume of the resulting mixed solution was dispensed into the mold using a syringe. The mold was heated at 60 °C in an oven until the water evaporated.

Supporting Information

Supporting Information is available from the Wiley Online Library or from the author.

Acknowledgements

The authors thank the Fundamental Research Funds for the Central Universities, Collaborative Innovation Center of Chemical Science and Engineering (Tianjin), Frontiers Science Center for New Organic Matter (Nankai University) and the Haihe Laboratory of Sustainable Chemical Transformations for financial support. The National Natural Science Foundation of China (Grant No. 22131008).

Conflict of Interest

The authors declare no conflict of interest.

Data Availability Statement

The data that support the findings of this study are available in the supplementary material of this article.

Keywords

multicolor, room temperature phosphorescence, single-phosphor, supramolecular assembly, β-cyclodextrin

Received: October 13, 2025
Revised: December 13, 2025
Published online: January 12, 2026

[1] C. J. C. Kenry, B. Liu, *Nat. Commun.* **2019**, *10*, 2111.
[2] B. S. Chang, J. Chen, J. S. Bao, T. L. Sun, Z. Cheng, *Chem. Rev.* **2023**, *123*, 13966.
[3] Z. X. Zhou, X. Y. Xie, Z. L. Sun, X. Wang, Z. F. An, W. Huang, *J. Mater. Chem. C* **2023**, *11*, 3143.
[4] X. Peng, P. Zou, J. Zeng, X. Wu, D. Xie, Y. Fu, D. Yang, D. Ma, B. Z. Tang, Z. Zhao, *Angew. Chem., Int. Ed.* **2024**, *63*, 202405418.
[5] J. Wang, B. Liang, J. Wei, Z. Li, Y. Xu, T. Yang, C. Li, Y. Wang, *Angew. Chem., Int. Ed.* **2021**, *60*, 15335.

[6] Y. Zhang, X. Chen, J. Xu, Q. Zhang, L. Gao, Z. Wang, L. Qu, K. Wang, Y. Li, Z. Cai, Y. Zhao, C. Yang, *J. Am. Chem. Soc.* **2022**, *144*, 6107.
[7] W. J. Zhao, Z. K. He, B. Z. Tang, *Nat. Rev. Mater.* **2020**, *5*, 869.
[8] H. Wang, H. Ma, N. Gan, K. Qin, Z. Song, A. Lv, K. Wang, W. Ye, X. Yao, C. Zhou, X. Wang, Z. Zhou, S. Yang, L. Yang, C. Bo, H. Shi, F. Huo, G. Li, W. Huang, Z. An, *Nat. Commun.* **2024**, *15*, 2134.
[9] X. Yan, H. Peng, Y. Xiang, J. Wang, L. Yu, Y. Tao, H. Li, W. Huang, R. Chen, *Small* **2022**, *18*, 2104073.
[10] Z. Yu, Y. Wu, L. Xiao, J. Chen, Q. Liao, J. Yao, H. Fu, *J. Am. Chem. Soc.* **2017**, *139*, 6376.
[11] S. Li, L. Fu, X. Xiao, H. Geng, Q. Liao, Y. Liao, H. Fu, *Angew. Chem., Int. Ed.* **2021**, *60*, 18059.
[12] Z. Wu, J. Nitsch, J. Schuster, A. Friedrich, K. Edkins, M. Loebnitz, F. Dinkelbach, V. Stepanenko, F. Würthner, C. M. Marian, L. Ji, T. B. Marder, *Angew. Chem., Int. Ed.* **2020**, *59*, 17137.
[13] C. W. Bunn, *Nature* **1948**, *161*, 929.
[14] H. E. Assender, A. H. Windle, *Polymer* **1998**, *39*, 4295.
[15] C. Chen, Z. Chi, K. C. Chong, A. S. Batsanov, Z. Yang, Z. Mao, Z. Yang, B. Liu, *Nat. Mater.* **2021**, *20*, 175.
[16] C. Tu, W. Wu, W. Liang, D. Zhang, W. Xu, S. Wan, W. Lu, C. Yang, *Angew. Chem., Int. Ed.* **2022**, *61*, 202203541.
[17] B. B. Ding, X. Ma, H. Tian, *Acc. Mater. Res.* **2023**, *4*, 827.
[18] Y. Zhang, W. Zhang, J. Xia, C. Xiong, G. Li, X. Li, P. Sun, J. Shi, B. Tong, Z. Cai, Y. Dong, *Angew. Chem., Int. Ed.* **2023**, *62*, 202314273.
[19] X. K. Ma, Y. Liu, *Acc. Chem. Res.* **2021**, *54*, 3403.
[20] N. Gan, X. Wang, H. Ma, A. Lv, H. Wang, Q. Wang, M. Gu, S. Cai, Y. Zhang, L. Fu, M. Zhang, C. Dong, W. Yao, H. Shi, Z. An, W. Huang, *Angew. Chem., Int. Ed.* **2019**, *58*, 14140.
[21] Y. Wen, H. Liu, S. Zhang, J. Cao, J. De, B. Yang, *Adv. Opt. Mater.* **2020**, *8*, 1901995.
[22] S. Yagai, S. Okamura, Y. Nakano, M. Yamauchi, K. Kishikawa, T. Karatsu, A. Kitamura, A. Ueno, D. Kuzuhara, H. Yamada, T. Seki, H. Ito, *Nat. Commun.* **2014**, *5*, 4013.
[23] S. Y. Jia, W. Fong, B. Graham, B. J. Boyd, *Chem. Mater.* **2018**, *30*, 2873.
[24] Z. Zhang, Y.-S. Wu, K.-C. Tang, C.-L. Chen, J.-W. Ho, J. Su, H. Tian, P.-T. Chou, *J. Am. Chem. Soc.* **2015**, *137*, 8509.
[25] D. J. Wang, T. Imae, *J. Am. Chem. Soc.* **2004**, *126*, 13204.
[26] Z. Z. Li, Q. Yue, H. C. Zhang, Y. L. Zhao, *Mater. Today* **2024**, *78*, 209.
[27] Y. J. Xie, Z. Li, *Chem.* **2018**, *4*, 943.
[28] H. K. Zhang, Z. Zhao, A. T. Turley, L. Wang, P. R. McGonigal, Y. Tu, Y. Li, Z. Wang, R. T. K. Kwok, J. W. Y. Lam, B. Z. Tang, *Adv. Mater.* **2020**, *32*, 2001457.
[29] J. Yu, Z. Sun, H. Ma, C. Wang, W. Huang, Z. He, W. Wu, H. Hu, W. Zhao, W.-H. Zhu, *Angew. Chem., Int. Ed.* **2023**, *62*, 202316647.
[30] Z. He, J. Song, C. Li, Z. Huang, W. Liu, X. Ma, *Adv. Mater.* **2025**, *37*, 2418506.
[31] B. Zhou, D. P. Yan, *Adv. Funct. Mater.* **2019**, *29*, 1807599.
[32] X. L. Zhou, X. Zhao, X. Bai, Q. W. Cheng, Y. Liu, *Adv. Funct. Mater.* **2024**, *34*, 2400898.
[33] L. M. Jin, Z. Y. Wang, W. Q. Mo, H. J. Deng, W. Hong, Z. G. Chi, *Angew. Chem., Int. Ed.* **2024**, *63*, 202410974.
[34] W. Feng, F. Li, Z. Jiang, C. Yue, G. Yin, N. Zhu, K. Zhang, T. Chen, W. Lu, *Angew. Chem., Int. Ed.* **2025**, *64*, 202505192.